Geomorphology 125 (2011) 109–121

Contents lists available at ScienceDirect

Geomorphology

journal homepage: www.elsevier.com/locate/geomorph

Catastrophic partial drainage of Pangong Tso, northern India and Tibet

Jason M. Dortch [a,*], Lewis A. Owen [a], Marc W. Caffee [b], Ulrich Kamp [c]

[a] Department of Geology, University of Cincinnati, Cincinnati, OH 45221, USA
[b] Department of Physics/PRIME Laboratory, Purdue University, West Lafayette, IN 47906, USA
[c] Department of Geography, The University of Montana, Missoula, MT 59812-1018, USA

ARTICLE INFO

Article history:
Received 30 April 2010
Received in revised form 25 August 2010
Accepted 27 August 2010
Available online 18 September 2010

Keywords:
Floods
Ladakh
Himalaya
^{10}Be dating
Strath terraces
Pangong Tso

ABSTRACT

Catastrophic partial drainage of Pangong Tso, one of the largest lakes in Tibet, is supported by the geomorphology of the Tangtse Valley, Ladakh, northern India and cosmogenic ^{10}Be nuclide ages of roche moutonnées, strath terraces, and a flood deposit downstream from the former spillway. The former spillway for Pangong Tso is ~20-m-high and likely allowed ~18 km^3 of water to drain catastrophically down the Tangtse Valley over a period of about 2 days sometime during the latest Pleistocene to early Holocene. The largest flood deposit, composed of imbricated granitic boulders up to 4.5 m in length, is present ~33 km downvalley of the spillway. These boulders have a cosmogenic ^{10}Be exposure age of 11.1 ± 1.0 ka, the age of the outburst flood. The minimum calculated discharge was ~110,000 m^3 s^{-1}. One set of strath terraces, upvalley of the flood deposit along the flood's drainage path, shows that the rate of fluvial incision 0.3 ± 0.1 mm y^{-1} during 122–10.5 ka increased to 1.5 ± 0.5 mm y^{-1} during 10.5 ka to the present. The temporal overlap of this increase in the rate of fluvial incision with the main flood deposit suggests that the flood was important in defining the incision along the Tangste valley. A second set of strath terraces shows little change in incision, from ~0.6–0.9 to ~0.9–1.4 mm y^{-1}, sometime between 18 and 27 ka. Roche moutonnées, upvalley from strath terraces, yield a cosmogenic ^{10}Be age of 35.8 ± 3.0 ka, defining the time when glaciers last occupied the Tangtse valley. However, the lack of glacial sediment along the Tangste valley suggests that the flood eroded glacial depositional landforms and sediments resulting in high sediment loads in the floodwater, which in turn increased fluvial incision to form strath terraces. Much of the eroded glacial sediment was subsequently redeposited as the main flood deposit. The catastrophic drainage of Pangong Tso may be the result of breaching of the Pangong–Tangste spillway during very high lake levels in a period of intensified monsoon (10.7–9.6 ka) and/or possibly the consequence of seismic activity along the Karakoram Fault that is associated with the initial formation of Pangong Tso.

1. Introduction

Catastrophic flooding associated with the sudden release of water impounded by glaciers, moraines, and landslides in high relief, high topography environments such as the Himalaya has a profound impact on the evolution of mountain landscapes, such as in the Himalaya (Hewitt, 1964, 1982; Ives, 1986; Vuichard and Zimmermann, 1987; Liu and Sharma, 1988; Yamada, 1993; Mool, 1995; Coxon et al., 1996; Reynolds, 1998; Richardson and Reynolds, 2000; Ballantyne, 2002, 2004; Korup and Montgomery, 2008; Seong et al., 2009). There are many large structurally controlled lakes in the Himalayan–Tibetan orogen, which potentially have significantly higher flood discharge and longer duration than more typical GLOFs. Such large events may affect the sediment budget and the distribution and preservation of landforms in high relief, high topography environments (Coxon et al., 1996). However, catastrophic flooding from bedrock dam failure is not common so its impact on mountain landscapes has not been fully assessed. In this paper, we examine evidence of a paleo-flood produced by the failure of a bedrock dam including: its deposit, resultant landforms, and the impact on the landscape development of the region.

Our study is centered in the Tangtse valley in the Pangong Range of the Transhimalaya. In the Tangtse valley, a series of flood deposits and strath terraces are present together with many well-preserved alluvial fans, lacustrine deposits, and roche moutonnées (Figs. 1 and 2). Our study focuses on examining these landforms and determining their origins using geomorphic mapping, remote sensing imagery, and cosmogenic ^{10}Be exposure dating. The late Quaternary and Holocene geomorphic evolution of the Tangtse valley is complex; but through our analysis of the various landforms present (in particular flood deposits and strath terraces), we are able to show that the valley's present morphology and distribution of landforms can be linked to a catastrophic outburst of water from Pangong Tso. Insights into quantitative aspects of erosion and deposition during this outburst flood were gained using Hydrologic Engineering Centers River Analysis System 4.0.

* Corresponding author. Now at Department of Chemical and Physical Sciences, University of Toronto Mississauga, Mississauga, ON L5L 1C6, Canada. Tel.: +1 905 8285397.
E-mail address: jason.dortch@utoronto.ca (J.M. Dortch).

0169-555X/$ – see front matter © 2010 Elsevier B.V. All rights reserved.
doi:10.1016/j.geomorph.2010.08.017

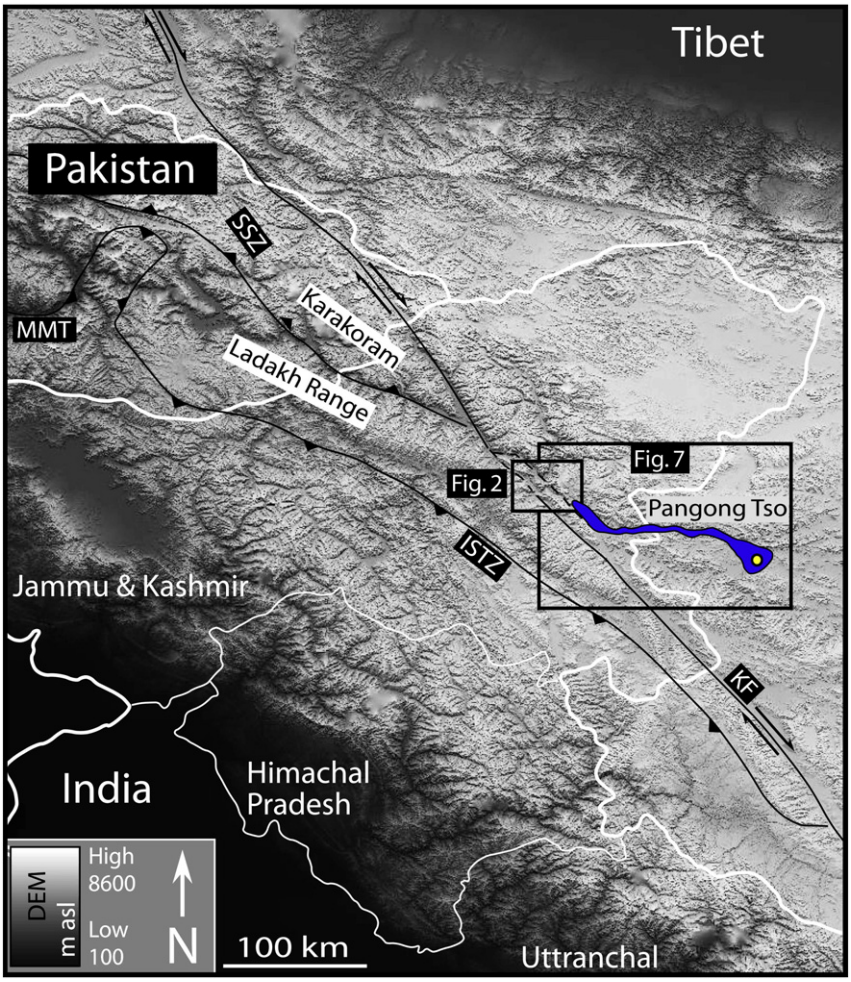

Fig. 1. SRTM DEM of the NW Indian Himalaya. The field area is highlighted by a box labeled "Fig. 2." Yellow dot marks the location of the sediment cores taken by Gasse et al. (1996).

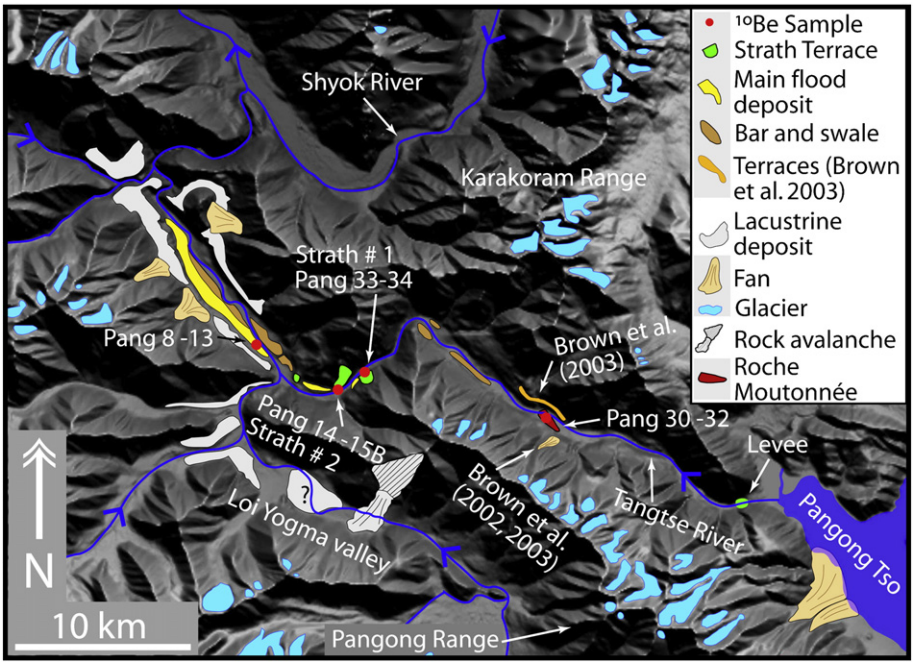

Fig. 2. Hillshade SRTM DEM with locations of mapped landforms. Contemporary glaciers in the Tangtse Valley are only present on the northern side of the Pangong Range.

2. Geologic setting

The study area is situated in the Pangong Range, which rises from valley floors at ~4000 m above sea level (asl) to peaks above 6000 m asl. The Pangong Range is composed of migmatitic gneiss and granitoids (Dunlap et al., 1998; Streule et al., 2009) and is bounded by the Pangong and Tangtse stands of the Karakoram Fault (Dunlap et al., 1998). Pangong Tso (Tso = Lake), one of the largest lakes in Tibet, traverses the eastern end of the study area and straddles the border of India and China. The northwestern basin of Pangong Tso is structurally controlled by oblique slip faulting along the Pangong strand of the Karakoram Fault (Dunlap et al., 1998; Searle et al., 1998; Chevalier et al., 2005; Searle and Richard, 2007). The Tangtse River to the northwest of Pangong Tso is the main drainage within the study area and drains into the Shyok River. Pangong Tso is in a closed basin (Shi et al., 2001), but it fed the Tangtse River during the Pleistocene. The Tangtse River now receives most of its waters from melting glaciers on the northern side of the Pangong Range and waters from the Loi Yogma valley (Fig. 2).

The climate of the region is semiarid, being in the rainshadow of the NW Himalaya (Bookhagen et al., 2005; Bookhagen and Burbank, 2006) but is nevertheless still dominated by precipitation from the south Asian summer monsoon (Gasse et al., 1996; Brown et al., 2003; Owen et al., 2006) that supplies between 250 and 500 mm of precipitation annually (Bookhagen and Burbank, 2006). Enhanced monsoon influence during times of increased insolation in the past likely played a dominant role in controlling lake levels for Pangong Tso and other lakes throughout Tibet (Gasse et al., 1996; Shi et al., 2001). Former high stands of Pangong Tso are recorded by stranded shorelines and terraces along the basin (Fontes et al., 1996).

3. Methods

3.1. Field methods

Landforms and sediments were identified and mapped in the field using topographic maps generated from 30-m resolution Advanced Spaceborne Thermal Emission and Reflection Radiometer (ASTER) digital elevation models (DEMs) and NASA WorldWind imagery (NASA, 2007).

Cosmogenic ^{10}Be extracted from quartz-rich bedrock and boulders was used to determine surface exposure ages of landforms. Two to six samples were collected from each landform. The samples were composed of rock fragments chipped (using a hammer and chisel) from the surface of the boulders or bedrock; the depth of the samples was ≤5 cm. The location, geomorphic setting, lithology, shape, and weathering characteristics of each sampled surface were recorded (Table 1). Topographic shielding was determined by measuring the inclination from the sampled surface to the surrounding horizon.

3.2. ^{10}Be surface exposure dating

We followed the procedures of Kohl and Nishiizumi (1992) for the extraction of Be from quartz. Dortch et al. (2009) summarized the entire process, including crushing, quartz isolation, chemistry, ignition, and preparation of an AMS cathode. ^{10}Be ages were calculated using the PRIME Laboratory Rock Age calculator (Ma et al., 2007; PRIME Laboratory, 2009) with the scaling factors of Stone (2000) and a ^{10}Be production rate of 4.5 atoms g^{-1} SiO_2^{-1} and a half-life of 1.36 ± 0.07 Ma (Nishiizumi et al., 2007).

Details of recalculating ^{10}Be ages from previous studies using the scaling scheme of Dunai (2000) are available in Appendix A. Corrections for geomagnetic field variations and erosion were not made (Appendix A). We refer the reader to Balco et al. (2008) and Owen et al. (2008) for more detailed discussions on this issue. ^{10}Be ages were analyzed using the mean square of weighted deviates (MSWD) method of McDougall and Harrison (1999) (Appendix A).

4. Landform descriptions and ages

Little previous work has been done on the geomorphology of the study area. However, Pant et al. (2005) described a 30- to 50-m thick deposit of lacustrine sediment in the Tangtse valley, and Brown et al. (2002, 2003) dated a flight of three river terrace surfaces and two faulted debris flows using cosmogenic ^{10}Be. Landforms in the Tangtse valley are described from Pangong Tso downvalley (Figs. 3 and 4).

4.1. Pangong Tso (Bangong Co)

Pangong Tso consists of five subbasins that are ~40-m deep and connected by sills that are at a depth of 1–2 m below the present lake surface, with the westernmost basin being the most saline (Fontes et al., 1996; Brown et al., 2003). Using δ^{18}O and δ^{13}C data and diatom and plankton fluctuations derived from sediment cores in the easternmost basin, Fontes et al. (1996) and Gasse et al. (1996) showed that the lake was more homogenous during high stands when it was actively draining through the spillway. Based on variance between δ^{18}O and δ^{13}C values, Fontes et al. (1996) suggested that the hydrological system opened abruptly and established a positive precipitation–evaporation balance between 1.3 ka and 11.0 ka (all radiocarbon ages are calibrated using CalPal-online). Gasse et al. (1996) suggested that three significant periods of increased precipitation caused by intensified monsoons occurred during the Holocene in the intervals 2.1–3.4 ka, 7.2–8.4 ka, and 9.6–11.0 ka.

Pangong Tso is presently at 4225 m asl, but former shorelines provide evidence of at least four higher lake level stands. Of particular note are shorelines and a terrace at the northern margin of the lake at 4280 ± 3 m asl (Norin, 1982; Pant et al., 2005). The terrace is composed of sand- to cobble-sized clasts that are alluvial fan deposits, reworked by littoral processes. Unfortunately, neither the shoreline nor terrace has been dated. Huang et al. (1989) and Li et al. (1991) reported a 79-m-high lake terrace, (4320 m asl) and Shi et al. (2001) dated this to between 35 and 45 ka (30,302 ± 685 and 40,602 ± 3320 ^{14}C years), suggesting that this terrace was likely formed during a high stand in a time of an intense monsoon precipitation.

High resolution Google Earth imagery shows two well-preserved shorelines on the NE side of Pangong Tso at ~4266 and ~4300 m asl. These shorelines were not accessible; accurate elevations could not be obtained or samples collected for dating.

4.2. Pangong Tso–Tangtse spillway

The Pangong Tso–Tangtse valley spillway is located at the northwestern end of Pangong Tso at 4247 ± 3 m asl (33.97° N., 78.04° E.) and comprises a series of low rising rockbars composed of marble. Three segmented rockbars trend west (~290°) perpendicular to the valley and follow the trend of outcropping bedrock (Fig. 3A). The top of the spillway is in the center of the valley and is at 4261 ± 3 m asl, rising to 4267 ± 3 m asl on the west on the flank of the Karakoram Range at approximately the same elevation as the lowest shoreline (4266 m asl). Collectively, the rockbars formed a paleospillway that was ~97-m wide and ~20-m-high.

Some segments of the spillway are fluvially eroded and exhibit fluted segments that trend parallel to the length of the valley. Most of the spillway surface (particularly the fluted segments) is smooth, water-worn, heavily fractured, and covered with sand and gravel. Several parts of the fluvially polished surfaces, ≤1 m in length, have been displaced, likely from frost heaving. Significant areas have a medium brown varnish, but exfoliated patches are light tan to white in color. Unfortunately, ^{10}Be dating could not be undertaken on the spillway because of the absence of quartz-rich lithologies.

Table 1
Details of ^{10}Be samples including location, ^{10}Be concentrations, and ages.[a]

Sample name	Latitude (DD)	Longitude (DD)	Elevation (M)	Thickness (cm)	Shielding correction	Uncorrected		Corrected[b]		PRIME Lab		
						^{10}Be atoms g^{-1} (10^4)	Error +/− atoms g^{-1} (10^4)	^{10}Be atoms g^{-1} (10^4)	Error +/− atoms g^{-1} (10^4)	Age std (ka)[c]	Age KN (ka)[d]	Age DZ (ka)[e]
Pang-8	34.047	78.154	3986	1	0.983	61.4	2.6	68.2	2.9	11.0 ± 0.9	11.0 ± 8.1	9.4 ± 0.7
Pang-9	34.047	78.154	3983	5	0.983	65.2	3.0	72.4	3.5	12.1 ± 1.0	12.0 ± 0.9	10.3 ± 0.8
Pang-10	34.047	78.154	3981	4	0.983	86.2	3.8	95.7	4.4	16.0 ± 1.3	15.6 ± 1.2	13.3 ± 1.1
Pang-11	34.047	78.155	3982	5	0.983	56.7	1.7	63.0	2.1	10.6 ± 0.8	10.5 ± 0.7	9.0 ± 0.7
Pang-12	34.047	78.154	3983	5	0.983	152.0	3.7	169.0	4.5	28.4 ± 2.0	26.4 ± 1.8	22.6 ± 1.6
Pang-13	34.047	78.154	3978	5	0.982	220.0	7.3	244.4	8.5	41.4 ± 3.1	36.8 ± 2.6	31.5 ± 2.4
Pang-14	34.024	78.195	4037	3	0.815	217.6	5.2	240.0	5.8	42.1 ± 3.0	37.3 ± 2.1	32.3 ± 7.0
Pang-15A	34.024	78.197	4016	3	0.915	92.3	5.1	101.9	5.6	17.9 ± 1.6	17.3 ± 1.4	15.0 ± 3.8
Pang-15B	34.024	78.197	4016	3	0.915	140.9	6.2	155.4	6.9	27.4 ± 2.2	25.6 ± 1.9	22.1 ± 5.6
Pang-30	34.009	78.302	4164	2	0.977	208.0	5.2	230.5	5.8	34.9 ± 2.5	31.7 ± 2.1	36.7 ± 1.9
Pang-31	34.009	78.302	4170	4	0.977	202.0	7.3	224.7	8.5	34.3 ± 2.6	31.3 ± 2.3	26.4 ± 2.0
Pang-32	34.009	78.303	4167	5	0.976	224.0	5.6	248.3	6.2	38.5 ± 2.8	34.7 ± 2.3	29.1 ± 0.6
Pang-33	34.032	78.209	4065	4	0.936	635.5	14.4	700.9	15.8	121.6 ± 8.8	106.3 ± 6.9	90.6 ± 22.9
Pang-34	34.033	78.210	4028	3	0.931	55.4	2.3	61.1	2.6	10.5 ± 0.8	10.6 ± 0.7	9.2 ± 2.2
KK98-1	34.006	78.299	4350	5	0.977	14.3	3.8	14.9	4.0	2.3 ± 0.6	2.5 ± 0.7	2.1 ± 0.6
KK98-3	34.006	78.299	4350	5	0.977	20.7	3.2	21.5	3.3	3.3 ± 0.6	3.6 ± 0.6	3.0 ± 0.5
KK98-4	34.006	78.299	4350	5	0.977	44.2	5.1	46.0	5.3	7.1 ± 1.0	7.3 ± 1.0	6.1 ± 0.9
KK98-5	34.006	78.299	4350	5	0.977	11.1	1.5	11.5	1.6	1.8 ± 0.3	1.9 ± 0.3	1.6 ± 0.2
KK98-6	34.006	78.299	4350	5	0.977	34.5	4.4	35.9	4.6	5.6 ± 0.8	5.8 ± 0.8	4.8 ± 0.7
KK98-7	34.006	78.299	4350	5	0.977	30.0	5.9	31.2	6.1	4.8 ± 1.0	5.1 ± 1.1	4.2 ± 0.9
KK98-8	34.006	78.299	4350	5	0.977	78.9	5.9	82.1	6.1	12.7 ± 1.3	12.6 ± 1.2	10.4 ± 1.1
KK98-14	34.006	78.299	4350	5	0.977	10.7	1.4	11.1	1.5	1.7 ± 0.3	1.9 ± 0.3	1.5 ± 0.2
KK98-15	34.006	78.299	4350	5	0.977	8.0	1.4	8.3	1.5	1.3 ± 0.2	1.4 ± 0.3	1.1 ± 0.2
KK97-41	34.006	78.299	4350	5	0.977	4.2	1.0	4.4	1.0	0.7 ± 0.2	0.8 ± 0.2	0.7 ± 0.2
KK97-41.5	34.006	78.299	4350	5	0.977	14.7	3.5	15.3	3.6	2.4 ± 0.6	2.6 ± 0.6	2.2 ± 0.6
KK97-36	34.006	78.299	4350	5	0.977	196.8	13.2	204.7	13.7	32.0 ± 3.0	29.3 ± 2.7	24.3 ± 2.4
KK97-37	34.006	78.299	4350	5	0.977	230.7	19.8	239.9	20.6	37.5 ± 4.1	33.8 ± 3.7	28.1 ± 3.2
KK97-38	34.006	78.299	4350	5	0.977	101.6	11.1	105.7	11.5	16.4 ± 2.1	16.0 ± 2.0	13.2 ± 1.8
KK97-39	34.006	78.299	4350	5	0.977	121.4	9.0	126.3	9.4	19.7 ± 2.0	18.8 ± 1.8	15.6 ± 1.6
KK97-40	34.006	78.299	4350	5	0.977	126.4	10.0	131.5	10.4	20.5 ± 2.1	19.6 ± 2.0	16.2 ± 1.8
KK98-9	34.006	78.299	4350	5	0.977	106.8	7.4	111.1	7.7	17.3 ± 1.7	16.7 ± 1.6	13.9 ± 1.4
KK98-10	34.006	78.299	4350	5	0.977	104.0	16.2	108.2	16.8	16.8 ± 2.9	16.3 ± 2.8	13.5 ± 2.4
KK98-11	34.006	78.299	4350	5	0.977	100.8	11.1	104.8	11.5	16.3 ± 2.1	15.9 ± 2.0	13.1 ± 1.8
KK98-12	34.006	78.299	4350	5	0.977	114.1	8.5	118.7	8.8	18.5 ± 1.9	17.8 ± 1.7	14.8 ± 1.6
KK98-13	34.006	78.299	4350	5	0.977	281.4	17.0	292.7	17.7	45.9 ± 4.2	40.0 ± 3.5	33.4 ± 3.2
KK97-24	34.008	78.311	4225	5	0.977	85.0	7.4	88.4	7.7	14.6 ± 1.6	14.3 ± 1.5	11.9 ± 1.4
KK97-26	34.008	78.311	4225	5	0.977	130.3	12.9	135.5	13.4	22.5 ± 2.7	21.3 ± 2.5	17.8 ± 2.2
KK97-27	34.008	78.311	4225	5	0.977	383.1	30.2	398.4	31.4	66.8 ± 7.0	58.3 ± 6.0	46.4 ± 5.1
KK97-28	34.008	78.311	4225	5	0.977	70.2	7.8	73.0	8.1	12.1 ± 1.6	11.9 ± 1.5	10.0 ± 1.4
KK97-29	34.008	78.311	4185	5	0.977	75.0	10.1	78.0	10.5	13.2 ± 2.0	13.0 ± 1.9	10.8 ± 1.7
KK97-30	34.008	78.311	4185	5	0.977	69.7	7.5	72.5	7.8	12.2 ± 1.6	12.1 ± 1.5	10.2 ± 1.4
KK97-33	34.008	78.311	4185	5	0.977	85.0	9.1	88.4	9.5	14.9 ± 1.9	14.6 ± 1.8	12.2 ± 1.6
KK97-34	34.008	78.311	4185	5	0.977	60.7	5.1	63.1	5.3	10.6 ± 1.1	10.6 ± 1.1	8.9 ± 1.0
KK97-35	34.008	78.311	4185	5	0.977	81.4	7.0	84.7	7.3	14.3 ± 1.6	14.0 ± 1.5	11.7 ± 1.3

[a] Assume zero erosion rate, standard pressure, and $\rho = 2.7$ g cm^{-3} for all samples.
[b] The isotope measurements were calibrated using KN Standard Be 0152 with a ^{9}Be/^{10}Be ratio of 8558E−15 atoms (c.f. Nishiizumi et al., 2007).
[c] Age calculated using the scaling model of Stone (2000) scaling scheme.
[d] Age calculated using the scaling model of Nishiizumi et al. (1989) scaling scheme.
[e] Age calculated using the scaling model of Desilets and Zreda (2003) scaling scheme.

4.3. Lacustrine deposits

Extensive lacustrine deposits are located in both the Tangtse and the Loi Yogma valleys (Fig. 2). The surface of the lacustrine deposits in the Tangtse valley forms a large bench at 4050 m asl on the western side of the valley. This bench is conformably covered with bouldery and sandy fanglomerate. A terrace at 3986 m asl is inset into the lacustrine sediment and is mantled with large (>4-m-diameter) imbricated boulders. Pant et al. (2005) described the lacustrine sediments above Tangtse Village as a 20–30-m thick succession of sediment that is dominantly composed of silt and clay. They suggested that the former lake high stand was formed by blockage of the Tangtse River behind terminal moraines formed as the valley glacier retreated. A second set of lacustrine deposits ~50-m thick is present immediately downvalley and forms a bench at 4070 m asl. These sediments are composed of sand and clay. Pant et al. (2005) suggested that they were deposited when a landslide blocked the Tangtse River near its confluence with the Shyok valley. Lacustrine sediments are absent upstream between strath terraces #1 and #2 and the Pangong Tso–Tangste spillway (Fig. 2).

Lacustrine deposits in the Loi Yogma valley are located at >4130 m asl and extend from the toe of a large landslide to the confluence with the Tangtse valley (Fig. 2). The contemporary river has incised the lacustrine deposit, but no boulders or imbricated deposits overly the lacustrine deposits as is the case in the Tangtse valley.

4.4. Roche moutonnées

A series of 2-4-m-high, NW-trending, whaleback-shaped phyllite knolls with steep/vertical leeward sides — pointing obliquely downvalley — are present ~10.5 km downvalley of the Pangong Tso–Tangste spillway (Figs. 3B and 4C). The surfaces of these landforms are smooth with numerous glacially beveled facets. These landforms are likely roche moutonnées formed when glaciers advanced down the Tangtse valley. Quartz veins 2–5-cm thick are present in the roche moutonnées, which have dark brown varnish and — where exfoliated — are pink to red in color. Depressions in the roche moutonnées are covered with medium to coarse sand. No till was located near the roche moutonnées or in the bottom of the Tangtse valley. Samples Pang-30, Pang-31, and Pang-32 were collected from quartz veins in these roche moutonnés that had dark brown varnish and that were flush with the host phyllite (Fig. 4D).

^{10}Be exposure ages from the roche moutonnées are 38.5 ± 2.8, 34.9 ± 2.5, and 34.3 ± 2.6 ka (Pang-30 to -32; Fig. 5), yielding an M_w of 35.8 ± 3.0 ka and an MSWD statistical indicator of 0.47. Although only three samples were dated, the tight clustering about the mean supports the view that the ^{10}Be exposure ages represent a geologic event.

4.5. Strath terraces

Two sets of strath terraces are present in the Tangtse valley (Fig. 3C). The contemporary Tangtse River is an underfit stream, and none of the strath terraces are currently being incised.

An ~100-m-high series of strath terraces in diorite bedrock (strath #1 in Fig. 2) are located ~24 km downvalley of the spillway. This strath terrace has a patchy dark brown desert varnish, is fluvially polished, and has scalloped surfaces. Two samples were collected at 15.5 m (Pang-33) and 52.5 m (Pang-34) above the contemporary river; higher strath terraces were not accessible (Table 2). These samples have ^{10}Be exposure ages of 10.5 ± 0.8 ka (Pang-33) and 121.6 ± 8.8 ka (Pang-34) (Figs. 4B and 5). We calculated the mean incision rates of 0.3 ± 0.1 and 1.5 ± 0.5 mm y^{-1} based on bracketing the strath terrace ages between 10.5–121.6 and 0.0–10.5 ka, respectively (Fig. 6B).

A second series of strath terraces rising to ~50 m above river and also composed of diorite (strath #2 in Fig. 2) are located ~1 km farther downvalley on the opposite side of the Tangtse River from strath terrace #1. These strath terraces have patchy dark brown rock varnish with polished and scalloped surfaces. Three samples were collected from this strath terrace: one at ~38 m (Pang-14) and two at ~25 m (Pang-15 A/B) above the river (Fig. 4A). They have ^{10}Be ages of 42.1 ± 3.0 ka (Pang-14), 17.9 ± 1.6 ka (Pang-15A), and 27.4 ± 2.2 ka (Pang-15B), respectively (Table 2). The discordant ages of Pang-15A and -15B may be the result of either transient debris on Pang-15A (shielding), or inheritance if Pang-15B was completely reset by fluvial erosion. The strath terrace surfaces are currently clear of debris, and both samples were collected from locally high surfaces to reduce the possibility of shielding (Fig. 4A). We suggest that transient debris only being deposited on the Pang-15A location is unlikely because the samples were collected ≤1 m apart. Alternatively, partial erosion of Pang-15B could account for its older age, but this is difficult to determine. To better represent the strath terraces incision history, we therefore present a range of incision rates: ~0.6–0.9 mm y^{-1} between Pang-14 and Pang-15A/B, and ~0.9–1.4 mm y^{-1} between Pang-15A/B and the contemporary river level.

4.6. River terraces

Brown et al. (2003) described a flight of three river terraces at ~40, 14, and 7 m above the Tangtse River and reported a mean ^{10}Be age of 7.2 ± 1.7 ka for the lower two river terraces (after subtracting the geologic background age of 2.0 ± 1.2 ka determined from boulders collected from the contemporary stream). Recalculated ^{10}Be ages (KK97-24 to -28) from the highest river terrace of Brown et al. (2003) provided ages that range from 12.1 ± 1.6 to 66.8 ± 7.0 ka (Fig. 5). The scatter of ^{10}Be ages from the ~40-m-high river terrace prevented the determination of an accurate age. Samples from the middle terrace (KK97-29 to -30) range in age from 12.2 ± 1.6 to 13.2 ± 2.0 ka, while ages range from 10.6 ± 1.1 to 14.9 ± 1.9 ka for the lower terrace (KK97-33 to -35). Brown et al. (2003) suggested that the highest river terrace was dissected and that the lower two terraces were formed during a brief period of valley incision. Our recalculated ^{10}Be ages show that the lower two terraces have ages that are indistinguishable. Following Brown et al. (2003), we combined the ages of the two lower terraces and took their M_w age as the most accurate estimate for the timing of river terrace formation. Statistical analysis showed no outliers; M_w is 12.5 ± 2.3 ka with a statistical indicator of 1.1. Compared to Brown et al. (2003), our age is older for two reasons: we have not subtracted an inherited component, and recently determined production rates effectively increase ages.

4.7. Alluvial fan surfaces

Brown et al. (2002, 2003) described an alluvial fan on the SW side of the Tangtse valley that has debris flow deposits inset into its surface and is offset by the Karakoram Fault. They presented ^{10}Be ages of ~1–2 ka for a debris flow deposit with a 2-m offset and 11.6 ± 1.8 ka for another debris flow deposit with a 40-m offset. Our recalculation of Brown et al.'s (2002, 2003) ^{10}Be exposure ages from the 40-m offset debris-flow ranges from 16.3 ± 2.1 to 45.9 ± 4.2 ka (samples KK97-38 and KK98-13; Fig. 5). Three outliers (KK98-13, and KK97-36 and -37) were identified through MSWD analysis, their higher exposure ages likely reflecting inheritance; the remaining seven samples have ^{10}Be ages from 16.3 ± 2.1 to 20.5 ± 2.1 ka with an M_w of 18.0 ± 1.5 ka and MSWD statistical indicator 0.52.

^{10}Be exposure ages from the 2-m offset debris flow deposit range from 1.3 ± 0.2 to 12.7 ± 1.3 ka (KK98-15 and KK98-8). Samples KK98-3, -4, -6, -7, and -8 were identified as outliers. Again, these all have higher ^{10}Be concentrations and our interpretation is that these samples have inherited ^{10}Be. The remaining four samples (KK98-1, -5, -14, and -15)

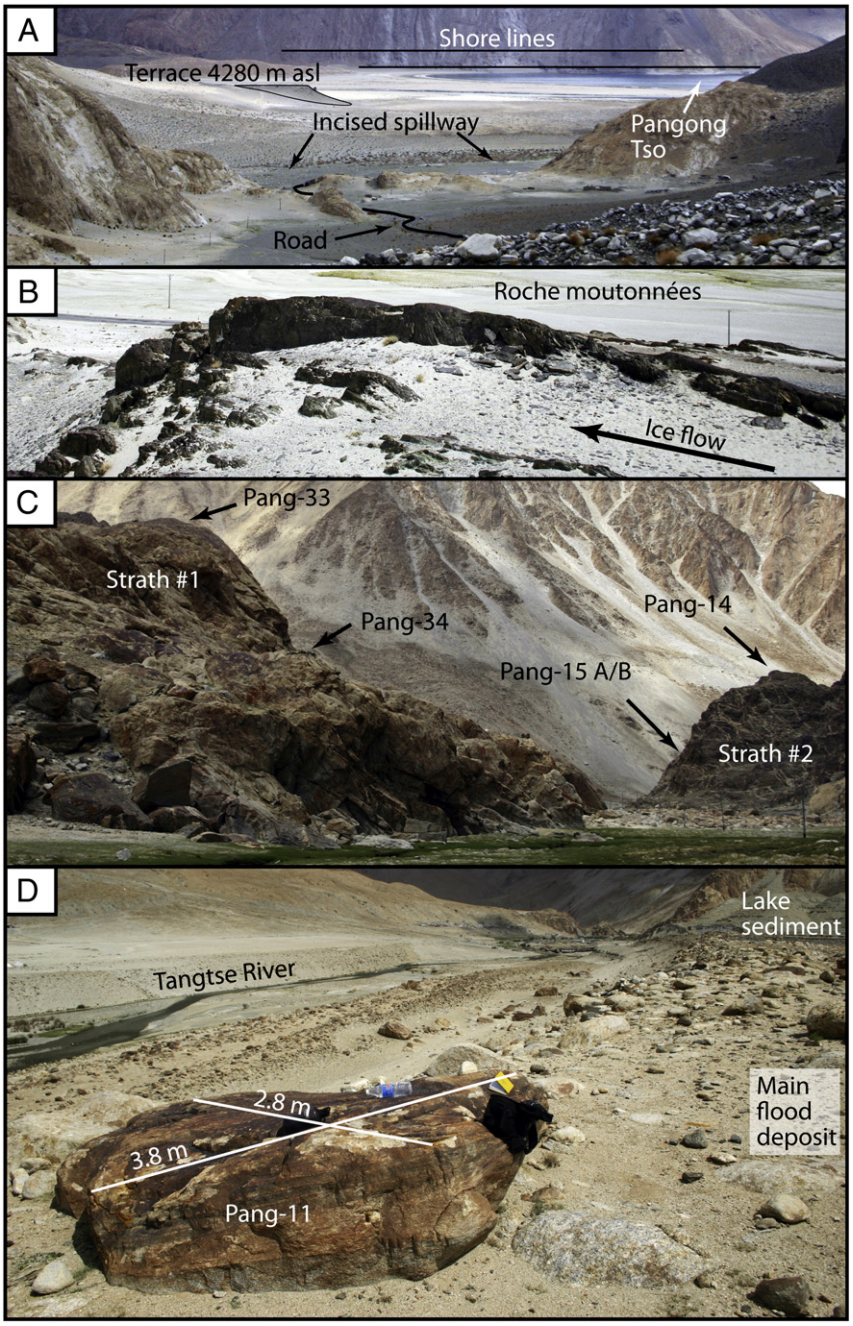

Fig. 3. Selected views of large landforms in the Tangtse Valley. (A) East view of the Pangong Tso–Tangtse spillway. Black arrows highlight the lowest elevations of the spillway. (B) North view across the Tangtse Valley of roche moutonnées partially covered by medium to coarse sand. (C) Southwest view of strath terraces #1 and #2 in the narrow part of the Tangtse Valley. D) Southeast view of the main flood deposit, with strath #3 in the background.

range from 2.3 ± 0.6 to 1.3 ± 0.2 ka with an M_w of 1.6 ± 0.3 ka and an MSWD statistical indicator of 0.90. Although our analysis does indicate the presence of a group, in this particular surface over half the samples had inheritance and were eliminated from the recalculated weighted average. Based on the amount of offset, however, we are confident that this surface is younger than the older fan, as expressed by the mean of the remaining four samples.

4.8. Flood deposit

The main flood deposit in the Tangtse valley begins at ~33 km downvalley from the Pangong Tso–Tangtse spillway (Fig. 2). Here, the Tangtse valley widens from ~0.38 to ~1 km. The flood deposit comprises subrounded boulders 1.0–4.5 m in length. The boulders are imbricated and occur as individuals or in clusters of 4 to 6 boulders (Fig. 4E and F). The boulders have patchy dark brown rock varnish and are slightly exfoliated. Samples Pang-8 to -13 were collected from boulders composed of phyllite and diorite. The lithology of the surrounding bedrock hillslopes, and the clasts that comprises local fans is diorite.

The main flood deposit is located on the southwestern side of the Tangtse valley and stretches for ~10.5 km (Fig. 3D). The main flood deposit is inset into lacustrine deposits and forms a large bench ~25 m above the river (3986 m asl from GPS or 3940 m asl from the ASTER DEM). Other parts of the flood deposit are present on the southeastern side of the Tangtse River and between strath terraces #1 and #2. Also, there is a 40 m long boulder with fluvial polish and concoidal fractures and imbricated boulders 1–17 m in length between strath terrace #2

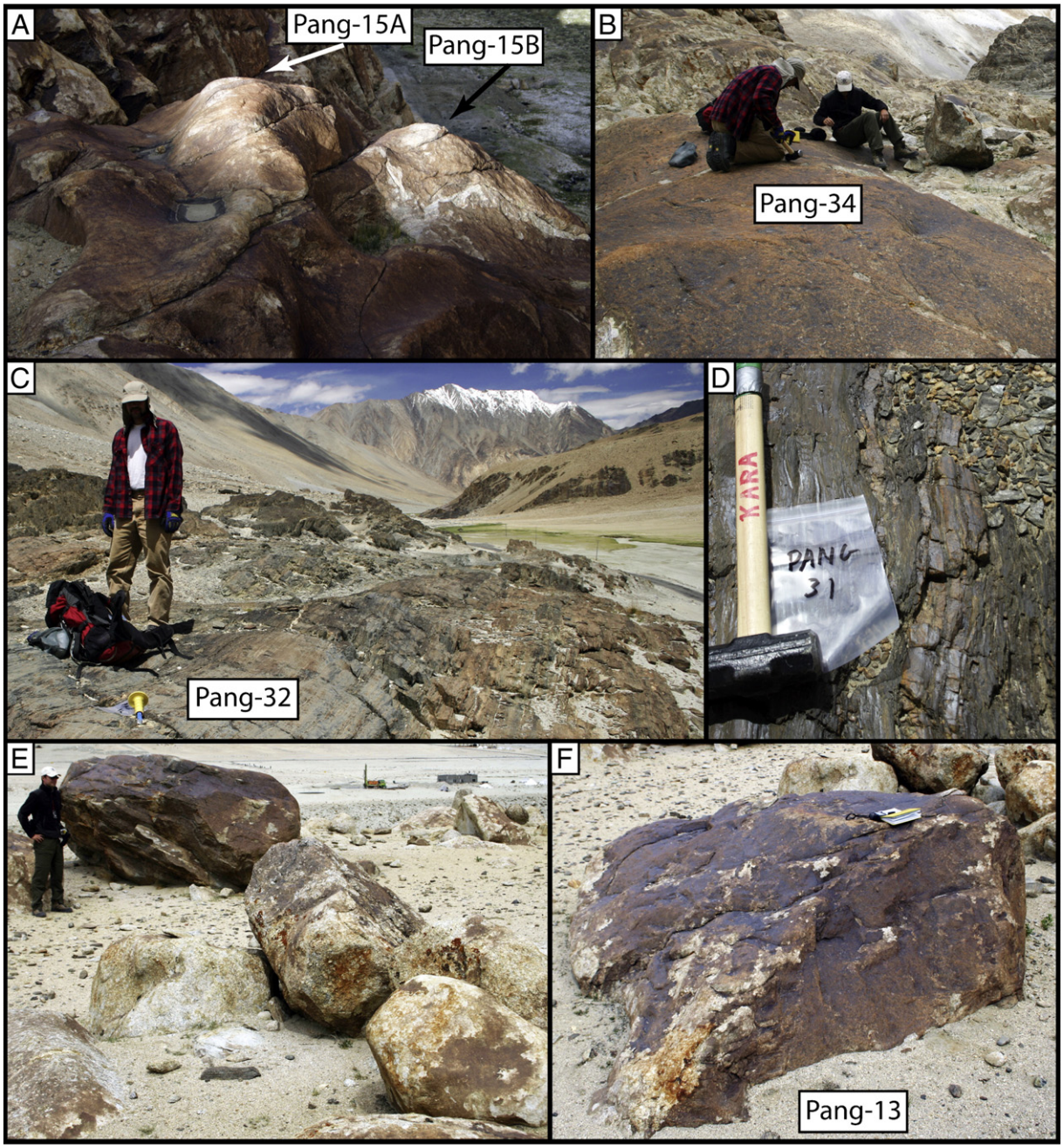

Fig. 4. Selected views of landform surfaces. (A) Fluvially polished surface of strath terrace #2 with large scallops and small potholes present. Samples are ~1 m apart for scale. B) Smooth polished surface of strath terrace #1. (C) On-trend view of glacially smoothed surface of roche moutonnées. Note the foliation of the phyllite unit and correlative outcrop across the valley. (D) Roche moutonnée sample location showing foliation. The light patch to the right of the hammer is a quartz vein with dark brown desert varnish. (E) View of the main flood deposit with large imbricated boulders. (F) Example of boulder sampled from the main flood deposit.

and the confluence with the Loi Yogma tributary valley (Coxon, pers. com; Appendix B, Fig. DS1). Extensive lacustrine sediments are present in the Loi Yogma tributary valley; however, both the ~65-m-high cut terrace and the flood deposit are absent.

^{10}Be exposure ages from the main flood deposit range from 41.4 ± 3.1 ka (Pang-13) to 10.6 ± 0.8 ka (Pang-11) (Fig. 5). Pang-10, -12, and -13 were identified as outliers through MSWD analysis. The remaining samples (Pang-8, -9, and -11) range between 10.5 and 12.1 ka and have an M_w of 11.1 ± 1.0 ka with an MSWD statistical indicator of 0.98. Because floods rework preexisting sediments and landforms, inherited boulder surfaces would be more common than typically found in other geologic settings, such as glacial deposits. Half the boulders we dated are identified as outliers, reflecting inheritance. All of the boulders we sampled had hard surfaces with no weathering rinds, suggesting that erosion is small on these samples. We suggest that the 11.1 ka age represents the real age of this flood.

5. Discussion

5.1. Velocity and discharge calculations

Sampled boulders from the flood deposit were used to reconstruct minimum velocities (V) of the flood using Eqs. (8) and (10) of Costa (1983):

$$V = 0.20 d_i^{0.455} \quad (1)$$

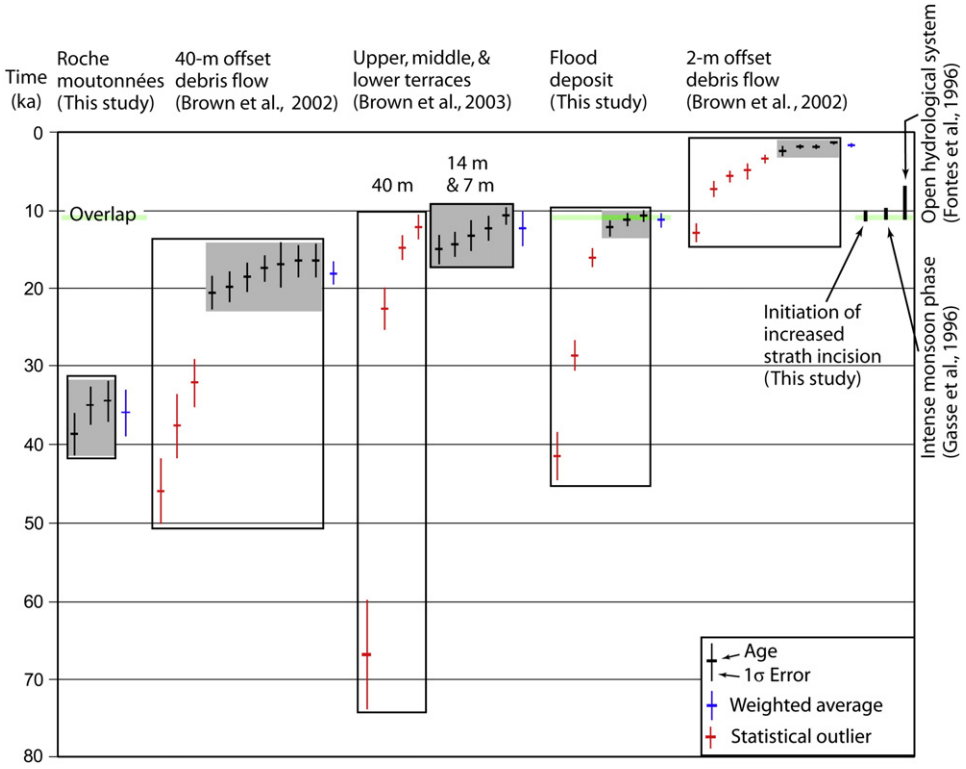

Fig. 5. ^{10}Be age plots of landforms in the Tangtse Valley arranged from oldest (left) to youngest (right). Dashed lines bracket the period when strath terrace incision rates increased significantly. Green bar highlights overlap of the timing of strath incision increase and flood and terrace deposition weighted mean ^{10}Be ages.

$$V = 0.18 d_i^{0.487} \quad (2)$$

Eq. (7) of Mears (1979):

$$V = \{[2Dg(1-\tan ß)(\cos ß)(\sigma-\rho_f)/\rho_f C_d]\}^{0.5} \quad (3)$$

and Eq. (7) of O'Connor (1993):

$$V = 0.29 d_i^{0.60} \quad (4)$$

These equations reconstruct the water velocities needed to overturn boulders based on the length of their intermediate axis (d_i) or D the average of the long, intermediate, and short axes; where σ is the specific gravity of the clasts (2.75 g cm^{-3}) and ß the gradient of the stream bed. The assumed constants include the frictional coefficient ($C_d = 0.6$) and fluid density ($\rho_f = 1.2$ g cm^{-3}) (Mears, 1979; Costa, 1983; O'Connor, 1993). The calculated boulder overturning velocity was determined where the flood deposits contained the largest boulders, that is, on the left bank of the Tangtse River (Fig. 2). The overturning velocity is a minimum as the methods of Mears (1979), Costa (1983), and O'Connor (1993) are limited to the size of boulders available for transportation by the flood event. Valley cross-sectional area (14,705 m^2) was determined in ArcMap (9.2) from ASTER DEMs using the highest boulder as a minimum estimate of the flood elevation.

Velocities needed to overturn the largest boulders are shown in Table 3; and our calculated values are 6.2 m s^{-1} (Costa, 1983: Eq. (8)), 7.3 m s^{-1} (Mears, 1979: Eq. (7)), 8.1 m s^{-1} (O'Connor, 1993: Eq. (7)), and 8.2 m s^{-1} (Costa, 1983; Eq. (10)), with an average of 7.5 m s^{-1} and a standard deviation of 0.9 m s^{-1}. The Tangtse valley has a cross-sectional area of ~14,700 m^2 where the main flood deposit is located (Appendix B Fig. DS5). The calculated mean discharge is ~110,000 ± 12,000 m^3 s^{-1} (uncertainty = standard deviation).

The contemporary Tangtse River is frozen in winter, and there are no direct measurements of stream discharge. However, the stream is small, only 1–2 m deep and we estimate the water velocity at ~1–2 m s^{-1}. At the location of the flood deposit boulders, where the ^{10}Be samples were collected, the modern river would have a cross-sectional area between 60 and 110 m^2, which yields discharge rates between ~50 and 200 m^3 s^{-1}. The calculated flood discharge far exceeds the contemporary discharge as well as any precipitation event in this semiarid setting (250–500 mm y^{-1}; Bookhagen and Burbank, 2006). The adjacent Loi Yogma valley does not contain the large imbricated boulders of the flood deposit like those in the Tangtse valley. Moreover, the Loi Yogma valley lacustrine sediments do not

Table 2
Details of strath terrace samples including relative order, incision height, and incision rate.

Sample name	Relative order	Elevation (M)	Error (m)	Height above river (m)	Incision height (m)	Incision error (m)	Age std (ka)	Incision rate (mm/y)[a]
Pang-14 (15A)	2	4037	5	38	13.4	6.4	42.1 ± 3.0	1.4 ± 0.3
Pang-15A	1	4016	4	24.6	24.6	4.6	17.9 ± 1.6	0.6 ± 0.3
Pang-14 (15B)	2	4037	5	38	13.4	6.4	42.1 ± 3.0	0.9 ± 0.2
Pang-15B	1	4016	4	24.6	24.6	4.6	27.4 ± 2.2	0.9 ± 0.5
Pang-33	2	4065	5	52.5	37	7.1	121.6 ± 8.8	0.3 ± 0.1
Pang-34	1	4028	5	15.5	15.5	5	10.5 ± 0.8	1.5 ± 0.5

[a] Elevation and ^{10}Be age errors are propagated quadratically.

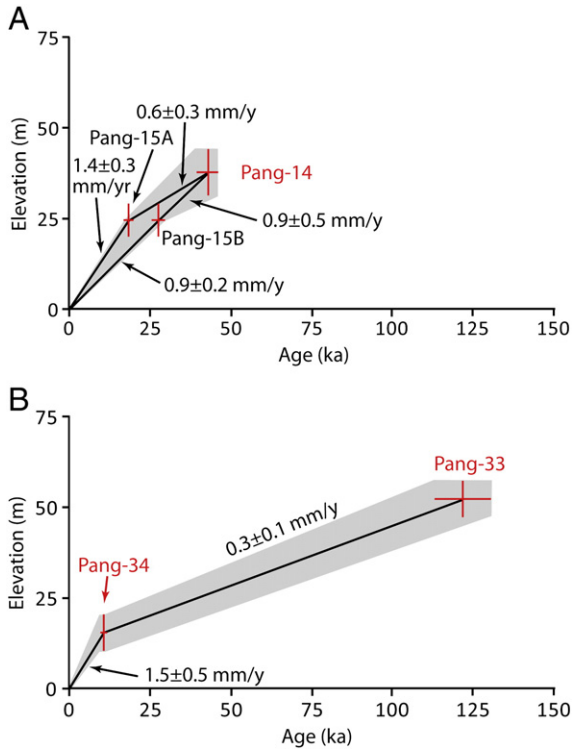

Fig. 6. Elevation versus age plots used to show strath terrace incision rates. The slope of the black line is the incision rate, and the shaded areas represent 1σ error. (A) Strath terrace #2 plot shows significant increase in incision at 22.7 ± 6.7 ka. (B) Strath terrace #1 plot shows significant increase in incision at 10.5 ± 0.8 ka.

contain a large erosional bench, thus precluding the Loi Yogma valley from contributing to the flood. No lake sediments are present between the roche moutonnées and the Pangong Tso–Tangtse spillway. We suggest that the absence of lacustrine sediments reduces the possibility that a glacial- or moraine-dammed lake was present in the valley. The tributary valleys of the Tangtse valley are small, and therefore, any moraine dams in these valleys would not have held sufficient volumes (»110,000 m^3) of water to transport >4-m-long boulders ~33 km downvalley. This supports the view that Pangong Tso is the only viable source for the floodwater to transport and deposit the large boulders.

Even though the lowering of the level of Pangong Tso was not large, the minimum volume of water that was discharged based on ASTER DEMs is 18,300 × 10^6 m^3 (Fig. 7). Reconstruction of former lake levels showed that all five sub-basins within Pangong Tso would still have been connected, which would enable water from all five lake basins to be discharged during one event (Fig. 7B and C). Moreover, the fact that the well-developed shorelines and the marble ridge at the Pangong Tso–Tangtse spillway are at similar elevation (4266 and 4267 m asl, respectively) suggests that the former lake level persisted for some time before the lake drained. The division of the potential volume of water released (18,300 × 10^6 m^3) by the average calculated discharge (~110,000 ± 12,000 m^3 s^{-1}) suggest the flood would have lasted ~46 ± 5 h.

5.2. HEC-RAS 4.0 model

Hydrologic Engineering Centers River Analysis System 4.0 (HEC-RAS) subcritical steady flow analysis was undertaken to model flow velocity, which can be used to elucidate erosion and deposition (U.S. Army Corps of Engineers, 2010). The channel geometry of the flood route was defined by 63 georeferenced cross sections imported from Hydrologic Engineering Centers Geo-River Analysis System 4.0 (HEC-GeoRAS). A roughness coefficient (n = 0.030) and expansion (0.5) and contraction (0.0) values were estimated based on the presence of sand, gravel, and boulders on channel bed, occasional cliff exposures as banks, and channel cross section (Barnes, 1967; Jarrett and Malde, 1987). We found a roughness coefficient of n = 0.030 to be the best fit with the contemporary Tangtse River valley morphology and landforms with those described and shown in Barnes (1967). Waythomas et al. (1996) used similar values to model a caldera outburst flood in Alaska. For our model, we assumed that the water surface of Pangong Tso was at the top of the spillway; the minimum discharge estimated from the boulder-turning moments was continuous; and that the spillway had its current morphology. Model data is available in the data repository (Appendix B Figs. DS2 to DS5 and Table-DS1). All elevations used in the HEC-RAS 4.0 and HEC-GeoRAS models were taken from the ASTER DEM because of the consistent ~40–50 m offset between DEM and GPS elevations.

The HEC-RAS 4.0 model enabled flow velocities through the Tangtse valley to be reconstructed based on discharge from the boulder turning-moment (110,000 ± 12,000 m^3 s^{-1}), flood volume (18,300 × 10^6 m^3), and valley geometry (Fig. 8, Appendix B DS2, and DS3). Water velocities could not be reconstructed without the HEC-RAS 4.0 model because of the lack of accurate water surface elevations. HEC-RAS 4.0 model water surface elevations are provided in Appendix B Fig. DS3 and Table DS1.

We use minimum flow velocities derived from turning moments for five boulders described by Coxon (pers. comm.) to verify the HEC-RAS 4.0 water velocities between cross sections 13,940–15,804 (the cross-sections are labeled and referred to by distance in meters from the beginning of the model geometry from the distal part of the flood deposit to the spillway; Appendix B Figs. DS2). Following the methods of Mears (1979), Costa (1983), and O'Connor (1993) provides a mean entrainment velocity of 16.2 ± 3.8 m s^{-1} (Appendix B Table DS2). The large variance in intermediate axis length (5–30 m) accounts for the large standard deviation (error) of the velocities. In spite of this, the average velocity from the five boulders fit well with the HEC-RAS 4.0 model (Fig. 8). Thus, we suggest that the HEC-RAS 4.0 model provides a reasonable estimate of water velocity during the flood event.

Most of the flood deposit occurs between cross-sections 5968 to 13,081. The modeled water velocities in the channel bottom for this reach range from 6.9 to 15.2 m s^{-1}, while for the left channel bank the velocities range from 4.1 to 8.4 m s^{-1}. Velocities for the left bank, where the flood boulders are located, fit well with the mean entrainment velocity of 7.5 m s^{-1}, estimated using the equations of O'Connor (1993) Costa (1983) and Mears (1979). The left bank water velocities show that boulder deposition likely occurred there while boulders in the center of the valley would continue to be transported through the fluvial system.

While floods can cause lateral incision into bedrock (Hartshorne et al., 2002), downcutting and vertical incision is controlled by channel bottom water velocities. Strath terraces #1 (cross-section 16,349) and #2 (cross-section 17,964) have modeled channel bottom velocities of 17.2 and 17.9 m^3 s^{-1}, respectively. The reduced valley cross-sectional area at the strath terrace locations results in a Venturi effect (increased water velocity through narrow passages), which enabled the fluvial system to incise its bedrock channel. Bedrock erosion via quarrying, macroabrasion, wear, chemical and physical weathering, and cavitation is enhanced during large floods (Whipple, 2004). Quarrying is the most efficient erosional process where it is active (Hancock et al., 1998). The HEC-RAS 4.0 model also shows that critical flow velocities are reached at the strath terrace locations (Appendix B Table DS2). Turbulent flow can create significant impacts from the large entrained boulders, which likely fractured the channel's bedrock. Moreover, the high water velocities enabled quarrying of the newly fractured blocks.

At the roche moutonnées' location (between cross-sections 28,800 and 29,563), the model provides subcritical channel bottom velocities that range from 9.6 to 12.9 m^3 s^{-1}. The flow velocities would enable

Table 3
Boulder size data, paleo-entrainment velocities, and discharge for the main flood deposit.

Sample name	a-axis (mm)	b-axis (mm)	c-axis (mm)	Entrainment velocity (Costa, 1983; Eq. (8)) (m/s)	Entrainment velocity (Costa, 1983; Eq. (10)) (m/s)	Entrainment velocity (Mears, 1979; Eq. (7)) (m/s)	Entrainment velocity (O'Connor, 1993; Eq. (7)) (m/s)	Mean entrainment velocity ± stdev (m/s)	Mean discharge based on individual boulders and cross-sectional area (m^3/s) (Fig. 8D)
Pang-8	2500	1400	800	4.9	6.1	5.4	5.6	5.51 ± 0.51	81097
Pang-9	4500	2000	1500	5.6	7.3	6.5	7.0	6.59 ± 0.72	96948
Pang-10	2250	2000	850	5.6	7.3	6.5	7.0	6.59 ± 0.72	96948
Pang-11	3800	2800	650	6.5	8.6	7.7	8.5	7.81 ± 0.99	114796
Pang-12	4300	3200	1050	6.8	9.2	8.2	9.2	8.35 ± 1.13	122778
Pang-13	4200	2900	900	6.6	8.7	7.8	8.7	7.95 ± 1.03	116841
Average of five largest boulders	3810	2580	990	**6.2**	**8.2**	**7.3**	**8.1**	**7.5 ± 0.91**	109662 ± 11970

the flood to entrain large glacial boulders and debris, but the subcritical flow conditions suggest that the flood water was not very turbulent, which would reduce the intensity and number of impacts on the roche moutonnées by entrained debris.

The modeled spillway velocity of 11.1 $m^3\ s^{-1}$ appears to be too low to have enabled significant incision into the marble bedrock. However, the significant fracturing of the marble into meter-sized blocks would enable quarrying to occur. Entrained sand and cobbles from fan and terrace debris lakeside of the spillway would provide the tools necessary to develop their fluvial streamline shape and the polish morphology on the rock bars present today.

5.3. Formation and reworking of landforms

The presence of roche moutonnées in the Tangtse valley shows that glaciers advanced downvalley from the northern slopes of the Pangong Range. Our ^{10}Be ages on the roche moutonnées place the age of glaciation at 35.8 ± 3.0 ka. This agrees reasonably well with glacial advances that have been dated in adjacent study areas, including a large moraine formed by Siachen Glacier in the Nubra valley dated to 45.2 ± 2.7 ka (Dortch et al., 2010) and a significant glacial advance at 45.5 ± 8.4 ka in the Puga valley (Hedrick et al., in press) south of the Ladakh Range, all during marine isotope stage (MIS) 3.

Alternatively, the roche moutonnée age (35.8 ± 3.0 ka) may reflect later partial exhumation of the roche moutonnées during the 11 ka flood event, the surface of the roche moutonnées having been eroded by the flood event. We suggest that flood-induced erosion is not significant because the roche moutonnées retain their whaleback form, still exhibit glacially beveled surfaces, and do not follow the trend of the valley. The preservation of the roche moutonnées is likely due to the valley width and the available sediment for flood erosion. The Tangtse valley is approximately five times wider at the roche moutonnées (~500 m wide) than at the strath terrace locations. This caused the HEC-RAS 4.0 model to show that water velocity, and subsequent erosive power, to be less at the roche moutonnées' location. Moreover, Roche moutonnées are subglacial features; therefore we suggest that the bulk of the glacial debris were likely deposited in front (down valley) of the roche moutonnées. Thus, they would not be available for entrainment and erosion of the roche moutonnées (i.e. less tools and subcritical flow results in less erosion).

Brown et al. (2003) suggested that the 14- and 7-m-high river terraces formed when increased precipitation from intensified monsoons caused Pangong Tso to overflow its bedrock spillway. Our recalculated M_w age of 12.5 ± 2.3 ka for these two lower river terraces overlaps the flood event age of 11.1 ± 1.0 ka. Gasse et al. (1996) and Fontes et al. (1996) showed that intensified monsoons occurred from 11.0 to 9.6 ka and that the Pangong Tso hydrological system opened abruptly at 11.0 ka, consistent with the flood deposit age. The age consistency between the river terraces and the flood deposit suggests that they were formed by the same event. These ages are also consistent with the suggestion by Brown et al. (2003) that the 40-m offset debris-flow (M_w 18.0 ± 1.5 ka) fan was incised by headward migration of a channel because of a lowering base level. Brown et al. (2003) attributed this lowering to the toe of the fan being cut by a debris-flow that formed the 14- and 7-m-high river terraces.

The accelerated incision of strath terrace #1 from 0.3 ± 0.1 mm y^{-1} (10.5–121.6 ka) to 1.5 ± 0.5 mm y^{-1} (0.0–10.5 ka) also overlaps with the age of the flood event (Fig. 5). Strath terrace #2 has little change in incision rate: from ~0.6–0.9 to ~0.9–1.4 mm sometime between 18 and 27 ka. These data suggest that the accelerated incision of strath terrace #1 was also a result of the flood event. The incision rate based on strath terrace #2 also changed, but the cause cannot be stated with certainty (Figs. 5 and 6). The contemporary Tangtse River is an underfit stream; therefore, the majority of the 15.5 m of incision (strath terrace #1) could be attributed to erosion during the flood event, likely enhancing the incision rate by >1.2 mm y^{-1}.

As our final considerations, the flood deposit is composed of diorite and phyllite boulders, but the surrounding bedrock hillslopes are composed only of diorite. This clearly shows that some of the boulders were transported from phyllite outcrops upvalley near the roche moutonnées. In addition, catastrophic drainage from Pangong Tso would have reworked most of the sediments along the flood of the Tangtse valley. ^{10}Be ages are similar between flood deposit outliers (16.0 ± 1.3 to 41.4 ± 3.1 ka), the 40 m offset fan (16–46 ka) and the "missing" glacial deposits near the roche moutonnées (≥35.8 ± 3.0 ka). Based on our data, a coherent scenario is one in which glacial and fan debris were flushed downvalley during the flood event. The entrained debris and large glacial boulders facilitated increased incision of the strath terraces and were deposited where the valley widens and the flow lost competency.

5.4. Dam failure

Determining the trigger and mode of failure for an ancient natural dam is difficult. Shi et al. (2001) suggested that the 4320-m-asl terrace was formed during a lake high-stand that was produced by increased monsoonal rainfall. Our ages for the flood deposit overlap with the suggested intensified monsoon phase of Gasse et al. (1996) and the timing of the opening of the Pangong Tso hydrological system suggested by Fontes et al. (1996). Pratt et al. (2002), Bookhagen et al. (2005, 2006), and Dortch et al. (2009) suggested that these intensified monsoon phases have played an important role in surficial processes throughout the NW Himalaya.

A significant increase in precipitation could have increased discharge over the spillway and cleft-water pressure within the spillway. The Pangong Tso–Tangste spillway is fractured and may

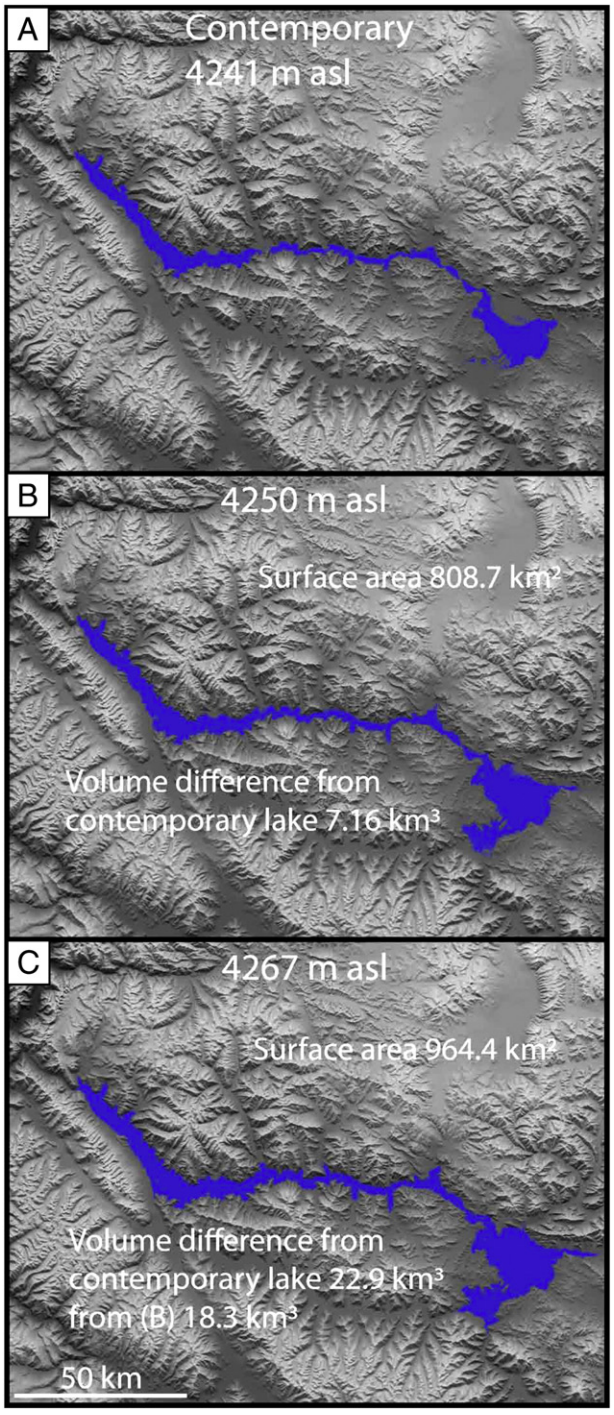

Fig. 7. Reconstruction of the water level for Pangong Tso water. (A) Contemporary lake consisting of five basins connected by 1–2 m deep sills. (B) Lake level at the bottom of the spillway after drainage. This shows that the lake basins were more strongly connected by 10–11 m deep sills. (C) Lake level at the top of the spillway before drainage. Here, the connecting sills are 27–28 m deep.

have been influenced by cleft-water pressure, much like a large landslide dam with angular clasts and jigsaw blocks. The potential water pathway through the spillway would likely have influenced how the spillway failed. Based on the water pathway through the spillway, its fractures and angularity, we suggest the Pangong Tso–Tangste spillway failed in a way similar to the failure of a remobilized landslide dam.

Seismic shaking, overtopping from increased precipitation, or a combination of the two may have triggered the failure of the spillway at 10.5 ka. Insight into the trigger of dam failure is provided by the former high lake level, which must have persisted long enough to form the well-developed shorelines (4266 m asl). Therefore, we suggest that increased water supply would have helped facilitate the catastrophic failure of the spillway, such as reducing the seismic shaking needed to cause the dam to fail, but it was probably not the sole factor in causing the flood. Gasse et al. (1996) and Fontes et al. (1996) could not preclude that tectonic activity along the Karakoram Fault may have caused fluctuations in the altitude of the Pangong Tso–Tangtse spillway, potentially inducing an opening at ~11.0 ka. Brown et al. (2003) suggested that tectonic activity, specifically the vertical component of the Karakoram Fault, did affect the spillway. Brown et al. (2002) also suggested that movement of the Karakoram Fault has a recurrence interval of 0.5 ka in the Tangtse valley. They speculate that a large earthquake breached the bedrock during a high stand of the lake.

5.5. Comparison with other floods

Comparison of the Pangong Tso–Tangste flood with other floods is difficult because failure of a bedrock spillway has not been widely studied and/or commonly reported. Fenton et al. (2004, 2006) report five catastrophic floods that occurred along the Colorado River due to the failure of lava dams. The largest of these dams was 366 m tall, had a peak discharge between 1,200,000 to 5,300,000 $m^3 s^{-1}$, and released 5000–11,000 $\times 10^6$ m^3 of water over 27–31 h. The peak discharge is an order of magnitude larger than the Pangong Tso flood (110,000 $m^3 s^{-1}$); however, the volume of water released (18,300 $\times 10^6$ m^3) and duration (~46 h) of the floods are comparable. The lower discharge of the Pangong Tso flood is due to the low spillway height (20 m), which limited hydrostatic pressure. Fenton et al. (2006) suggest that the short duration of the lava dam flood would have exerted less stream power compared to more sustained floods with lower discharges. However, the Tangtse River valley is in a region with a transport limited setting where old and well formed MIS-8 and MIS-6 deposits are preserved in most valleys (Owen et al., 2006; Seong et al., 2007; Dortch et al., 2010). The partial drainage of Pangong Tso is 10^2–10^3 times larger than contemporary flow and would have had significant impact not only on erosion, but also the remobilization and transportation of landforms and sediments within the valley.

The partial drainage of Pangong Tso can also be compared to other types of floods in the Himalaya, including glacial lake outburst floods (GLOF) and catastrophic landslide dam failures. In particular, GLOF have been well documented with discharges of up to 30,000 $m^3 s^{-1}$ (Richardson and Reynolds, 2000). Seong et al. (2009), for example, described three GLOF deposits, composed of imbricated boulders 5–13 m in diameter in the Braldu valley in the central Karakoram, and estimated flood discharges of 6400 ± 1400 $m^3 s^{-1}$, 22,400 ± 7800 $m^3 s^{-1}$, and 36,500 ± 8400 $m^3 s^{-1}$. Coxon et al. (1996) determined that the catastrophic drainage of Glacial Lake Batal released 1.5 km^3 of water with a discharge of 21,000–27,000 $m^3 s^{-1}$. However, these rates are significantly lower than our minimum calculated discharge rate of ~110,000 $m^3 s^{-1}$.

The discharge, duration, and volume of water released from Pangong Tso exceed all natural dams reported by Costa and Schuster (1988); whose summary of catastrophic failures includes 26 earth and rock fill dams, 12 landslide dams, 8 moraine dams, and 11 glacier dams form around the world. In a more recent world wide compilation of the largest floods by Fenton et al. (2006), the partial drainage of Pangong Tso would rank #30. Bedrock dam failures, such as the Pangong Tso–Tangtse event, can create some of the largest catastrophic floods recorded and dominate the geomorphic development of a valley. The reworking of landforms and sediments because of the flood event likely destroyed the glacial record in the Tangtse valley. Moreover, the high discharge likely caused significant bedrock

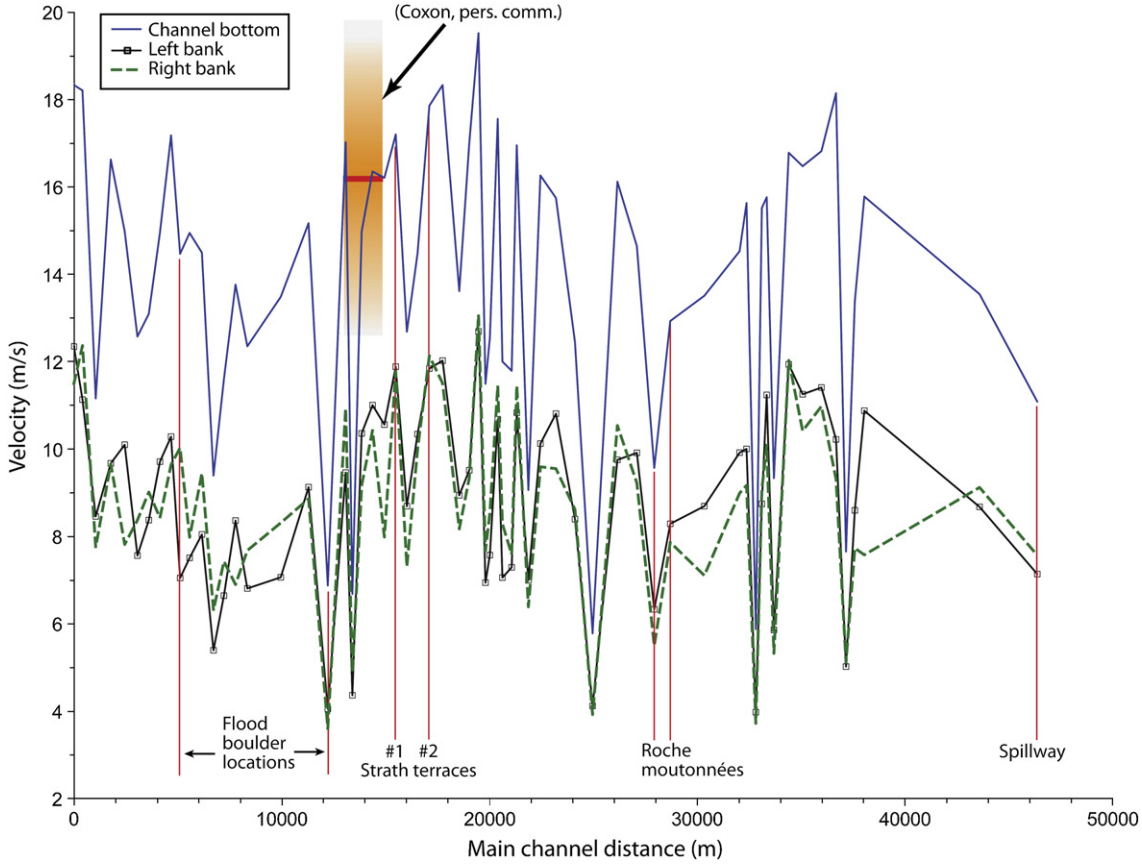

Fig. 8. HEC-RAS modeled flow velocity based on calculated discharge from boulder entrainment. X-axis is labeled with respect to distance in meters from the start of the modeled section of the Tangtse Valley. Locations of interest are labeled with red vertical lines. Data from Coxon (pers. comm.) used to verify the model is marked by small red bar (velocity) and orange gradient (standard deviation).

incision. However, this catastrophic flood is also a formative process that created the ~11-ka flood deposit, tall strath terraces, and large erosional benches that dominate the landscape today.

6. Conclusions

The partial drainage of Pangong Tso resulted in a catastrophic flood that likely released ~18.3 km^3 of water, reworking many landforms in the Tangtse valley, and resulting in significant incision. A high lake level likely initiated overtopping of a fractured marble spillway and increasing cleft water pressure. Initiation of the flood was possibly due to seismic activity along the Karakoram Fault in combination with an intensified monsoon phase at 9.6–11.0 ka leading to an abrupt opening of the hydrological system at 11.0 ka. The flood deposit is located ~33 km downvalley and is composed of imbricated granitic boulders of up to 4.5 m in diameter and 11.1 ± 1.0 ka in age. The minimum calculated discharge at the flood deposit location is estimated to have been ~110,000 $m^3\ s^{-1}$. One set of strath terraces shows that the rate of fluvial incision increased approximately fivefold since 10.5 ka. The age of the flood deposit overlaps with the timing for the initiation of increased fluvial incision of bedrock at ~10.5 ka. Roche moutonnées, upvalley from strath terraces, yielded a cosmogenic ^{10}Be age of 35.8 ± 3.0 ka; but there are no glacial deposits in the Tangtse valley. In detail, the broad range of ages of boulders that compose the flood deposit suggests that the missing glacial debris and other landforms upvalley were reworked during the flooding event, enabling increased fluvial incision as recorded by the strath terraces, and that they have been preserved as the flood deposit.

The large boulders that comprise the flood deposit provide evidence that catastrophic floods can move significant debris across faults zones and that they can affect sediment budgets. The dominance of the flood event on the contemporary geomorphology of the Tangtse valley shows that, in a semiarid environment where rates of erosion and fluvial incision may be low, older landforms can be remobilized and altered significantly during one short-lived event. In such cases, determining rates of processes and ages of older events, and even recognizing them, can be difficult. Moreover, catastrophic events have significant effects on landform preservation and morphostratigraphic correlation.

Acknowledgements

Jason Dortch thanks the Department of Geology at the University of Cincinnati for supporting this study as part of his doctoral research. He also thanks Sigma Xi, the American Alpine Club, and the University Research Counsel for funding this study, Susan Ma for helping calculate our ^{10}Be ages and recalculate ages from other studies, and Dr. Jonathan Remo for help with HEC-RAS modeling. We thank two anonymous reviewers and Richard Marston for their constructive and helpful comments on our manuscript. Special thanks to Dr. Peter Coxon who provided important feedback and additional data that greatly improved this manuscript.

Appendix A. Supplementary data

Supplementary data to this article can be found online at doi:10.1016/j.geomorph.2010.08.017.

References

Balco, G., Briner, J., Finkel, R.C., Rayburn, J., Ridge, J.C., Schaefer, J.M., 2008. Regional beryllium-10 production rate calibration for late-glacial northeastern North America. Quaternary Science Reviews 4, 93–107.

Ballantyne, C.K., 2002. Paraglacial geomorphology. Quaternary Science Reviews 21, 1935–2017.

Ballantyne, C.K., 2004. Paraglacial landsystems. In: Evans, D.J. (Ed.), Glacial Land Systems. Edward Arnold, London, pp. 432–461.

Barnes Jr., H.H., 1967. Roughness characteristics of natural channels. Water-Supply Paper, 1849. U.S. Geological Survey, Box 25425, Denver, CO. 219 pp.

Bookhagen, B., Burbank, D.W., 2006. Topography, relief, and TRMM-derived rainfall variations along the Himalaya. Geophysical Research Letters 33, L08405.

Bookhagen, B., Thiede, R.C., Strecker, M.R., 2005. Late Quaternary intensified monsoon phases control landscape evolution in the northwest Himalaya. Geology 33, 149–152.

Brown, E.T., Bendick, R., Bourlés, D.L., Gaur, V., Molnar, P., Raisbeck, G.M., Yiou, F., 2002. Slip rates of the Karakorum Fault, Ladakh, India, determined using cosmic ray exposure dating of debris flows and moraines. Journal of Geophysical Research 107, 2192 doi:10.1029/2000JB000100.

Brown, E.T., Bendick, R., Bourlés, D.L., Gaur, V., Molnar, P., Raisbeck, G.M., Yiou, F., 2003. Early Holocene climate recorded in geomorphological features in western Tibet. Palaeogeography, Palaeoclimatology, Palaeoecology 199, 141–151.

Chevalier, M.L., Ryerson, F.J., Tapponnier, P., Finkel, R.C., Van Der Woerd, J., Haibing, L., Qing, L., 2005. Slip-rate measurements on the Karakoram Fault may imply secular variations in fault motion. Science 307, 411–414.

Costa, J.E., 1983. Paleohydraulic reconstruction of flash-flood peaks from boulder deposits in the Colorado Front Range. Geological Society of America Bulletin 94, 986–1004.

Costa, J.E., Schuster, R.L., 1988. The formation and failure of natural dams. Geological Society of America Bulletin 100, 1054–1068.

Coxon, P., Owen, L.A., Mitchell, W.A., 1996. A late Quaternary catastrophic flood in the Lahul Himalaya. Journal of Quaternary Science 11, 495–510.

Desilets, D., Zreda, M., 2003. Spatial and temporal distribution of secondary cosmic-ray nucleon intensities and applications to in-situ cosmogenic dating. Earth and Planetary Science Letters 206, 21–42.

Dortch, J., Owen, L.A., Haneberg, W.C., Caffee, M.W., Dietsch, C., Kamp, D.U., 2009. Nature and timing of large landslides in the Himalaya and Transhimalaya of northern India. Quaternary Science Reviews 28, 1037–1054.

Dortch, J., Owen, L.A., Caffee, M.W., 2010. Quaternary glaciation in the Nubra and Shyok valley confluence, northernmost Ladakh, India. Quaternary Research 74, 132–144.

Dunai, T.J., 2000. Scaling factors for production rates of in situ produced cosmogenic nuclides; a critical reevaluation. Earth and Planetary Science Letters 176, 157–169.

Dunlap, W.J., Weinberg, R.F., Searle, M.P., 1998. Karakoram fault zone rocks cool in two phases. Geological Society of London 155, 903–912.

Fenton, C.R., Poreda, R.J., Nash, B.P., Webb, R.H., Cerling, T.E., 2004. Geochemical discrimination of five Pleistocene lava-dam outburst-flood deposits, Grand Canyon. Journal of Geology 112, 91–110.

Fenton, C.R., Webb, R.H., Cerling, T.E., 2006. Peak discharge of a Pleistocene lava-dam outburst flood in Grand Canyon, Arizona, USA. Quaternary Research 65, 324335.

Fontes, J.C., Gasse, F., Gilbert, E., Derbyshire, E., 1996. Holocene environmental changes in Lake Bangong Basin (western Tibet); Part 1, Chronology and stable isotopes of carbonates of a Holocene lacustrine core. Palaeogeography, Palaeoclimatology, Palaeoecology 120, 25–47.

Gasse, F., Fontes, J.C., Van Campo, E., Wei, K., 1996. Holocene environmental changes in Bangong Co basin (western Tibet). Part 4: Discussion and conclusions. Paleogeography, Paleoclimatology, Paleoecology 120, 79–92.

Hancock, G.S., Anderson, R.S., Whipple, K.X., 1998. Beyond power; bedrock river incision process and form. In: Tinkler, K.J., Whol, E.E. (Eds.), Rivers over rock, fluvial processes in bedrock channels: American Geophysical Union Monograph, 107, pp. 35–60.

Hartshorne, K., Hovius, N., Dade, B., Slingerland, R.L., 2002. Climate-driven bedrock incision in an active mountian belt. Science 297, 2036–2038.

Hedrick, K.A.H., Seong, Y.B., Owen, L.A., Caffee, M.W., Dietsch, C. In press. Towards defining the transition in style and timing of Quaternary glaciation between the monsoon-influenced Greater Himalaya and the semi-arid Transhimalaya of Northern India. Quaternary International, doi:10.1016/j.quaint.2010.07.023.

Hewitt, K., 1964. A Karakoram ice dam. Industrial Journal of Water and Power Development Authority (Pakistan) 5, 18–30.

Hewitt, K., 1982. Natural dams and outburst floods of the Karakoram Himalaya. In: Glen, J. W. (Ed.), Hydrological Aspects of Alpine and High Mountain Areas. International Association of Hydrological Sciences, Publication no. 138 pp. 259–269.

Huang, C.X., Zhang, Q.S., Liu, F.T., 1989. A preliminary study of paleovegetation and paleoclimate in the later period of late Pleistocene in Bangongcuo Lake region of Xizang. Journal of Natural Resources 4, 247–253 (In Chinese).

Ives, J.D., 1986. Glacial Lake outburst floods and risk engineering in the Himalaya. Occasional Paper, 5. International Center for Integrated Mountain Development, Kathmandu, Nepal.

Jarrett, R.D., Malde, H.E., 1987. Paleodischarge of the late Pleistocene Bonneville flood, Snake River, Idaho, computed from new evidence. Geological Society of America Bulletin 99, 127–134.

Kohl, C.P., Nishiizumi, K., 1992. Chemical isolation of quartz for measurements of in-situ-produced cosmogenic nuclides. Geochimica et Cosmochimica Acta 56, 3583–3587.

Korup, O., Montgomery, D.R., 2008. Tibetan plateau river incision inhibited by glacial stabilization of the Tsangpo gorge. Nature 455, 780–786.

Li, S.J., Zhen, B.X., Jiao, K.Q., 1991. Prelimanary research on lacustrine deposit and lake evolution on the slope of west Kunlun Mountains. Scientia Geographica Sinica 4, 306–314.

Liu, C., Sharma, C.K. (Eds.), 1988. Report on the First Expedition to Glaciers and Glacier Lakes in the Pumqu (Arun) and Poiqu (Bhote-Sun-Kosi) River Basins, Xizang (Tibet), China: Sino-Nepalese Investigation of Glacier Lake Outburst Floods in the Himalaya. Science Press, Beijing, China, p. 192.

Ma, X.Z., Li, Y.K., Bourgeois, M., Caffee, M.W., Elmore, D., Granger, D., Muzikar, P., Smith, P., 2007. Webcn: a web-based computation tool for in situ-produced cosmogenic nuclides. Nuclear Instruments & Methods in Physics Research, Section B, Beam Interactions with Materials and Atoms 259, 646–652.

McDougall, I., Harrison, T.M., 1999. Geochronology and Thermochronology by the 40Ar/39Ar Method. Oxford University Press, Oxford, p. 269.

Mears, A.I., 1979. Flooding and sediment transport in a small alpine drainage basin in Colorado. Geology 7, 53–57.

Mool, P.K., 1995. Glacier lake outburst floods in Nepal. Journal of Nepal Geological Society 11, 273–280.

National Aeronautics and Space Administration (NASA), 2007. Land Processes Distributed Active Archive Center, Earth Observing Data Gateway. http://edcimswww.cr.usgs.gov/pub/imswelcome/2007.

Nishiizumi, K., Arnold, J.R., Klein, J., Kohl, C.P., Lal, D., 1989. Cosmic ray production rates of ^{10}Be and ^{26}Al in quartz from glacially polished rocks. Journal of Geophysical Research 94, 17907–17915.

Nishiizumi, K., Imamura, M., Caffee, M.W., Southon, J.R., Finkel, R.C., McAninch, J., 2007. Absolute calibration of ^{10}Be AMS standards. Nuclear Instruments and Methods in Physics Research, Section B, Beam Interactions with Materials and Atoms 258B, 403–413.

Norin, E., 1982. Reports from the scientific expedition to the north-western provinces of China under the leadership of Dr. Sven Hedin, The sino-swedish epedition. Suppl. 54. I. Geography. 5 Sven Hedin Central Asia Atlas, Memoir on Maps, vol. 1II, facs. l: The Pamirs, Kunlun, Karakorum and Chan T'ang region, p. 61.

O'Connor, J.E., 1993. Hydrology, hydraulics, and geomorphology of the Bonneville flood. Geological Society of America Special Paper, 274. 83 pp.

Owen, L.A., Caffee, M.W., Bovard, K.R., Finkel, R.C., Sharma, M.C., 2006. Terrestrial cosmogenic nuclide surface exposure dating of the oldest glacial successions in the Himalayan orogen: Ladakh Range, northern India. Geological Society of America Bulletin 118, 383–392.

Owen, L.A., Caffee, M.W., Finkel, R.C., Seong, B.Y., 2008. Quaternary glaciations of the Himalayan–Tibetan orogen. Journal of Quaternary Science 23, 513–532.

Pant, R.K., Phadtare, N.R., Chamyal, L.S., Juyal, N., 2005. Quaternary deposits in Ladakh and Karakoram Himalaya: a treasure trove of the paleoclimate records. Current Science 88, 1789–1798.

Pratt, B., Burbank, D.W., Heimsath, A., Ojha, T., 2002. Impulsive alluviation during early Holocene strengthened Monsoons, central Nepal Himalaya. Geology 30, 911–914.

PRIME Laboratory, 2009. PRIME Laboratory rock age calculator. https://www.physics.purdue.edu/ams/rosetest/Rkversion1/rockpara.php; and an important note concerning ^{10}Be results at http://www.physics.purdue.edu/primelab/News/news0907.php.

Reynolds, J.M., 1998. High-altitude glacial lake hazard assessment and mitigation: a Himalayan perspective. In: Maund, J.G., Eddleston, M. (Eds.), Geohazards in Engineering Geology. : Engineering Geology Special Publications, 15. Geological Society of London, pp. 25–34.

Richardson, S.D., Reynolds, J.M., 2000. An overview of glacial hazards in the Himalayas. Quaternary International 65 (66), 31–47.

Searle, M.P., Richard, J.P., 2007. Relationships between right-lateral shear along the Karakoram fault and metamorphism, magmatism, exhumation and uplift: evidence from the K2-Gasherbrum, Pangong ranges, north Pakistan and Ladakh. Geological Society of London 164, 439–450.

Searle, M.P., Dewey, J.F., Dunlap, W.J., Strachan, R.A., Weinberg, R.F., 1998. Transpression tectonics along the Karakoram fault zone, northern Ladakh; constraints on Tibetan extrusion. Geological Society Special Publications, Continental Transpressional and Transtensional Tectonics 135, 307–326.

Seong, Y.B., Owen, L.A., Bishop, M.P., Bush, A., Clendon, P., Copland, L., Finkel, R., Kamp, U., Shroder, J.F., 2007. Quaternary glacial history of the central Karakoram. Quaternary Science Reviews 26, 3384–3405.

Seong, Y.B., Bishop, M.P., Bush, A., Clendon, P., Copland, L., Finkel, R., Kamp, U., Owen, L.A., Shroder, J.F., 2009. Landforms and landscape evolution in the Skardu, Shigar and Braldu Valleys, central Karakoram Mountains. Geomorphology 103, 251–267.

Shi, Y., Yu, G., Liu, X., Li, B., Yao, T., 2001. Reconstruction of the 30–40 ka BP enhanced Indian monsoon climate based on geological records from the Tibetan Plateau. Paleogeography, Paleoclimatology, Paleoecology 169, 69–83.

Stone, J.O., 2000. Air pressure and cosmogenic isotope production. Journal of Geophysical Research 105, 23753–23759.

Streule, M.J., Phillips, R.J., Searle, M.P., Waters, D.J., Horstwood, M.S.A., 2009. Evolution and chronology of the Pangong metamorphic complex adjacent to the Karakoram Fault, Ladakh: constraints from thermochronology, metamorphic modeling and U–Pb geochronology. Journal of the Geological Society of London 166, 919–932.

U.S. Army Corps of Engineers, 2010. Hydrologic Engineering Centers River Analysis System 4.0 (HEC-RAS 4.0). http://www.hec.usace.army.mil/software/hec-ras/index.html2010.

Vuichard, D., Zimmermann, M., 1987. The catastrophic drainage of a moraine-dammed lake, Khumbu Himal, Nepal: cause and consequences. Mountain Research and Development 7, 91–110.

Waythomas, C.F., Walder, J.S., McGimsey, R.G., Neal, C.A., 1996. A catastrophic flood caused by drainage of a caldera lake at Aniakchak Volcano, Alaska, and impacts for volcanic hazard assessment. Geological Society of America Bulletin 108, 861–871.

Whipple, K.X., 2004. Bedrock rivers and the geomorphology of active orogens. Annual Reviews of Earth and Planetary Sciences 32, 151–185.

Yamada, T., 1993. Glacier lakes and their outburst floods in the Nepal Himalaya. Water and Energy Commission Secretariat, Kathmandu, Nepal, p. 37.